THE JOURNAL OF BIOLOGICAL CHEMISTRY VOL. 286, NO. 11, pp. 9514–9525, March 18, 2011

ApoA-II Directs Morphogenetic Movements of Zebrafish Embryo by Preventing Chromosome Fusion during Nuclear Division in Yolk Syncytial Layer*[S]

Received for publication, April 16, 2010, and in revised form, December 27, 2010 Published, JBC Papers in Press, January 6, 2011, DOI 10.1074/jbc.M110.134908

Ting Zhang[‡], Shaohua Yao[‡], Ping Wang[‡], Chaoran Yin[‡], Chun Xiao[‡], Meilin Qian[‡], Donghui Liu[§], Lemin Zheng[§], Wentong Meng[‡], Hongyan Zhu[‡], Jin Liu[‡], Hong Xu[‡1], and Xianming Mo[‡2]

From the [‡]Laboratory of Stem Cell Biology, State Key Laboratory of Biotherapy, West China Hospital West China Medical School, Sichuan University, Chengdu 610041, China and the [§]Institute of Cardiovascular Sciences and Key Laboratory of Molecular Cardiovascular Sciences, Ministry of Education, Peking University Health Science Center, Beijing 100191, China

The high density lipoprotein (HDL) represents a class of lipid- and protein-containing particles and consists of two major apolipoproteins apoA-I and apoA-II. ApoA-II has been shown to be involved in the pathogenesis of insulin resistance, adiposity, diabetes, and metabolic syndrome. In embryo, *apoa2* mRNAs are abundant in the liver, brain, lung, placenta, and in fish yolk syncytial layer (YSL), suggesting that *apoa2* may perform a function during embryonic development. Here we find out that *apoa2* modulates zebrafish embryonic development by regulating the organization of YSL. Disruption of *apoa2* function in zebrafish caused chromosome fusing, which strongly blocked YSL nuclear division, inducing disorders in YSL organization and finally disturbing the embryonic epiboly. Purified native human apoA-II was able specifically to rescue the defects and induced nuclear division in zebrafish embryos and in human HeLa cells. The C terminus of apoA-II was required for the proper chromosome separation during nuclear division of YSL in zebrafish embryos and in human HeLa cells. Our data indicate that organization of YSL is required for blastoderm patterning and morphogenesis and suggest that apolipoprotein apoA-II is a novel factor of nuclear division in YSL involved in the regulation of early zebrafish embryonic morphogenesis and in mammalian cells for proliferation.

Apolipoproteins, including apoA-I, apoA-II, apoA-IV, apoB, apoC-I, apoC-II, apoC-III, apoC-IV, and apoE, are macromolecular complexes synthesized mainly in liver and intestine and play essential roles in lipid uptake and transport in vertebrates (1–3). They bind to lipids to form chylomicrons, very low density lipoprotein (VLDL), low density lipoprotein (LDL), and high density lipoprotein (HDL)[3] and transport lipid to various tissues through the circulation system. In addition to their function in lipid metabolism, several apolipoproteins play critical roles in embryonic and ontogenic development and tissue regeneration (4, 5).

The fish lipoprotein HDL is highly similar to most mammalian HDLs and contain two major apolipoproteins: the 28 kDa apolipoprotein and 14 kDa apolipoprotein (6–8). The 14 kDa apolipoprotein is identified as a second major component of HDL from Japanese eel, common carp, pufferfish, orange-spotted grouper, grass carp, and fathead minnow (9). Recent data show that fish 14 kDa apolipoprotein is orthologous to mammalian HDL apoA-II (10), which has been shown to involve pathogenesis of insulin resistance, adiposity, diabetes, and metabolic syndrome. The *apoa2* mRNAs are abundant in the liver, lung, placenta, brain (6, 11, 12) in embryos. In some fish species, *apoa2* also expresses in heart. In addition, *apoa2* has been found to express in YSL in embryos (9), suggesting that *apoa2* may perform functions during embryonic gastrulation. The previous data indicate that yolk lipids are taken up by the fish YSL, where they are assembled into lipoproteins for releasing into the perisyncytial space (13). Apolipoprotein gene expression and lipoprotein secretion by teleost fish YSL indicate that this extraembryonic temporary structure could be the functional counterpart of the anterior visceral endoderm (AVE) of higher vertebrates. This investigation of the YSL provides information for understanding detailed AVE function.

Embryonic gastrulation generates the three primary germ layers including ectoderm, mesoderm, and endoderm during vertebrate development. The morphogenetic movements of gastrulation have been well described (14) and the epiboly is the first morphogenetic movement of teleost gastrulation. Prior to epiboly, the zebrafish embryo undergoes meroblastic cleavage to generate a blastoderm cap on top of a single large yolk cell (15). The blastoderm consists of a superficial cell layer known as the enveloping layer (EVL), and a deep cell layer (DEL). Then, blastomeres at the boundary with the yolk cell collapse to release their nuclei into the yolk cell to form the YSL (15, 16). YSL formation usually begins after the 512-cell stage and is completed by the end of the 1000 cell phase during zebrafish embryonic development (15, 16). The nuclei in YSL (YSN)

* This work was supported by the National Basic Research Program of China (2009CB941200) and the Nature Science Foundation of China (to H. X. (30771228) and to X. M. (30771227)).

[S] The on-line version of this article (available at http://www.jbc.org) contains supplemental Figs. S1–S6.

[1] To whom correspondence may be addressed: Keyuan 4 Lu, High Tech. Distric. Chengdu, 610041 China. E-mail: xuhongm@yahoo.com.

[2] To whom correspondence may be addressed: Keyuan 4 Lu, High Tech. Distric. Chengdu, 610041 China. Tel.: 00862885164017; Fax: 00862885164047; E-mail: xmingmo@scu.edu.cn.

[3] The abbreviations used are: HDL, high density lipoprotein; YSL, yolk syncytial layer; YSN, nuclei in yolk syncytial layer; AVE, anterior visceral endoderm; EVL, enveloping layer; DEL, deep cell layer; MO, morpholino oligonucleotides; RD, rhodamine dextran; AV, animal-vegetal; hpf, h post-fertilization.

undergo three to five rounds of divisions and then cease mitosis at the sphere stage (16, 17). At this stage, the YSL contains several hundred YSN that can be subdivided into two main groups according to their position within the YSL (16, 18). External YSN (eYSN) form a marginal band of YSN located in front of the enveloping cell layer. During YSL organization, some of the eYSNs move toward the vegetal pole (epiboly movements), whereas others recede from the marginal zone and undergo convergence and extension (CE) movements (18, 19). By contrast, internal YSN (iYSN) are located below the blastoderm and EVL and primarily undergo CE movements (18). The epiboly and convergence and extension movements of YSN constitute the main events of YSL patterning that play crucial roles in embryonic patterning and morphogenesis (17, 19).

A set of genes have been identified for YSN patterning including squint (*sqt*), casanova (*cas*), GATA-binding protein 5 (*gata5*), hematopoietically expressed homeobox (*hhex*), retinol-binding protein 4 (*rbp4*), and metaxin 1 (*mtx1*) (20–26). Those genes perform functions in regulating nuclear movements in YSL. In contrast, there is little data to show that nuclear division plays a role in YSN patterning to modulate gastrula movements during embryonic development. In the present study, we show that the zebrafish *apoa2* gene expresses high levels in the ventral portion of YSL, regulates YSN division, modulates the spatial organization of nuclei in YSL and then regulates the embryonic patterning in zebrafish. Disruption of *apoa2* induces severe defects in embryonic gastrulation. In addition, we also show that apoA-II is required for nuclear division in human HeLa cells. Our data present a novel finding that apoA-II plays an essential role in nuclear division in YSL for embryonic patterning in zebrafish and in human cells for proliferation.

EXPERIMENTAL PROCEDURES

Embryos—Zebrafish (*Danio rerio*) were raised and maintained according to standard procedures (27). Embryos were raised at 28.5 °C and staged as described (28).

Molecular Cloning, Sequencing, and Phylogeny Analysis—Zebrafish *apoa2* (LOC: 570408) was searched for and identified from the NCBI core nucleotide program. We designed coding region primers for PCR cloning according to XM_693887 for *apoa2* (sense-primer: CACTTTTTGTACACTTACTA-ACAAT and antisense-primer: AAATACATGGTT-GAGGGAGT). The resultant PCR products were ligated into pGem-T easy vector, and cDNA sequences were confirmed. The relevant sequences were analyzed for multiple sequence alignments using DNAMAN6.0. Different percentages of amino acid identity were recorded after individual sequence comparisons. A phylogeny tree was constructed based on the amino acid sequences using DNAMAN6.0.

In Situ Hybridization—apoa2 antisense RNA probe was synthesized from its cDNA with a digoxygenin RNA labeling kit (Roche) corresponding to the entire coding sequence region (426 bp) of the *apoa2* gene, using SP6 RNA polymerase (Promega). Whole-mount *in situ* hybridization was carried out as previously described (29). In brief, embryos were permeabilized with proteinase K (10 μg/ml, Promega) and hybridized overnight at 65 °C with the DIG-labeled antisense probes. After several washes at high stringent temperature, NBT/BCIP (Roche) staining was performed according to the manufacturer's instructions.

Microinjection—Injection into the yolk of zebrafish embryos was performed at the 1-cell or 1k-cell stage. Antisense morpholino oligonucleotides were purchased from Gene Tools (Philomath). These MOs were designed complementary to the 5′ sequence near the translational initiation site of *apoa2* (*apoa2* MOs) with the sequences: *apoa2* MO1, 5′- GAATGAGAGC-GAATGTCAGCTTCAT-3′ (targets 5′ sequence spanning the start codon); and *apoa2* MO2, 5′-TGTTAGTAAGTGTA-CAAAAAGTGAG-3′ (directed against the sequence 5′ of the UTR to the start codon). Sequences were as follows: standard control MO, 5′-CCTCTTACCTCAGTTACAATTTATA-3′. Capped *apoa2* mRNA was synthesized from its cDNA subcloned in the pcDNA3.1(+) vector using mMACHINE T7 Ultra Kit (Ambion). SYTOX Green, which acts to specifically label nuclei, was injected into yolk at 1k-cell stage, at 50 μM, as described (21).

Immunofluorescence Staining of Whole-mount Embryos and HeLa Cell Whole-mount Embryo Staining—Zebrafish embryos were collected and fixed overnight in 4% PFA (in PBS), washed twice in PBS and once in ultrapure water for 5 min, permeabilized in acetone at −20 °C for 7 min, and then washed once in ultrapure water and twice in PBS for 5 min. The embryos were treated with 3% BSA in PBS for 30 min and then soaked in anti F-actin antibody or anti α-tubulin antibody (Millipore) overnight at 4 °C. The embryos were washed for 2 h with frequent changes of PBS and treated with secondary antibody at a concentration of 1:800 (Molecular Probes/Invitrogen) for 1 h. Embryos were rinsed twice in PBS for 5 min and stained with DAPI (1:5000; Molecular Probes/Invitrogen). HeLa cell staining: The cells were fixed for 15 min in 4% PFA (in PBS), washed three times with PBS for 5 min, incubated with 3% BSA and 0.5% Triton in PBS for 20 min, and washed once in PBS for 5 min. The cells were incubated with anti-H3pS10 antibody (Millipore cat. 06-570), α-tubulin (Millipore cat.04-1117) antibody diluted 1:1000, or γ-tubulin antibody diluted 1:5000 (Sigma T6557) in 3% BSA in PBST for 1 h at 37 °C, washed three times with PBS, and then incubated with secondary antibodies diluted 1:1000 in PBST with 3% BSA for 1 h at 37 °C and washed three times with PBS.

Total RNA Isolation and Quantitative RT-PCR—Total RNAs of 100 embryos at different stages, including 4-cell, sphere, 30% epiboly, shield, tail-bud, and 24 h post-fertilization (hpf) were isolated. The total volume for each reaction was 20 μl using the PrimeScript RT-PCR kit (TaKaRa DRR014A). All resultant cDNAs were used as templates for PCR with ExTaq DNA polymerase (TaKaRa). One pair of primers (*apoa2* sense: CTT-GCACTCCAAGTGTCAGTG, *apoa2* antisense: TGAAA-ATACATGGTTGAGGGA) were synthesized (Invitrogen) used to express levels during embryogenesis. As a positive control for RT-PCR analysis, actin primers (β-actin sense: TGTGGCCCTG-GACTTCGAGCAG and β-actin antisense: TAGAAGCACTTC-CTGTGGACGA) were designed to amplify a 474-bp fragment (GenBank™ accession number BC045846.1). A series of PCR reactions were performed with β-actin primers to determine the

template concentration and to provide a quantitative internal control for PCR reaction efficiency under the same reaction conditions as *apoa2*.

Construction of apoa2 Mutants—Six mutants of zebrafish *apoa2* were designed on the basis of conserved domain analysis and generated by PCR. The C-terminal deletion mutants included MC77, MC46, and MC36, which were missing 64, 95, and 105 amino acids, respectively. The N-terminal deletion mutants comprised MN20, MN47, and MN79, which were missing 19, 46, and 78 amino acids, respectively. Capped *apoa2* mutant mRNA was synthesized as described above.

Cell Migration Analysis by UV-mediated Photoactivation—Embryos were injected and imaged at bud stage for analysis of convergence and extension as described (30).

Isolation of HDL from Human Plasma—The density of the plasma was adjusted to 1.3 g/ml with KBr, and normal saline (density is 1.006 g/ml) was layered over the adjusted plasma to form a discontinuous NaCl/KBr density gradient. The tubes loaded with sample and gradient were placed in a P40ST rotor of Toshiba ultracentrifuge (model: CP70MX). The tubes were centrifuged at 350,000 rpm for 3.5 h at 10 °C. The HDL layer was collected. The purity was evaluated by Western blotting using anti-apoAI polyclonal antibody (DiaSorin), and the quantity was measured by nephelometer-Dimension XPand (Dade Behring, Germany).

Electroelution of ApoAII from HDL—1 mg of protein of HDL was delipidated and subjected to SDS-PAGE under nonreducing conditions. The gel was stained with Coomassie Blue, and the band of apoAII was cut and electroeluted for 5 h in a dialysis bag. The protein in the dialysis bag was re-dialyzed in PBS buffer. The dialyzed apoAII was lyophilized and resuspended in 0.1 M Tris-HCl (pH 7.4) with 0.1 M NaCl, 1 mM EDTA, and 3 M guanidinium chloride, and then dialyzed in PBS before use.

Analysis of Chromosome Morphology—HeLa cells were treated with colchicine (Sigma) at 37 °C for 4 h. Cells in suspension were centrifuged for 8 min at 800 × *g*, and the supernatant was removed. The prewarmed hypotonic solution was added. The cell pellet was resuspended by pipetting up and down with a Pasteur pipette and incubated for 20 min at 37 °C. 10 to 15 drops of methacarn (~0.5 ml) were added to the cell suspension from a Pasteur pipette and mixed. The cells were centrifuged, and the supernatant was aspirated. Methacarn was added, and the cells were resuspended with a pipette and left for 10 min at room temperature. The cells were centrifuged, and the supernatant was aspirated. 1% paraformaldehyde was added to cell pellets to form a somewhat cloudy suspension. 15–20 μl of the fixed cells were dropped onto slides from a height of ~37.5 cm and allowed to air dry. The slides were washed 5 min in PBS and stained with DAPI.

Fluorescence in Situ Hybridization of Whole-mount Embryos—Zebrafish embryos were harvested at the sphere stage and were fixed in 4% paraformaldehyde at 4 °C overnight, washed one time in PBS for 5 min, then incubated in acetone at −20 °C for 5 min and washed three times in PBS for 5 min each wash. 100 μg/ml RNase I were added to the zebrafish embryos, incubated 1 h at 37 °C, and washed two times in PBS for 5 min each. The embryos were incubated in protease K (0.1 μg/ml) for 1 min at room temperature and washed three times in PBS for 5 min each. Embryos were fixed in 4% paraformaldehyde for 20 min and washed three times in PBS for 5 min each. Embryos were passed through a dehydrating series of 70, 80, and 100% ethanol for 5 min each. Embryos were denatured for 10 min in 70% formamide/2× SSC (pH 7.0), 72 °C. Embryos were passed through a dehydrating series of 70, 80, and 100% ethanol for 5 min each. The Cy3-labeled (GGGTTA)7 oligomer probe (Invitrogen) was added to the pretreated embryos and hybridized for at least 16 h at 37 °C. The embryos were washed three times in 30% formamide in 2× SSC, then five changes of 2× SSC, all at 45 °C, and then counterstained with DAPI.

Serum-free Cellular Growth Assay—HeLa cells were plated onto chamber slides in DMEM medium containing 10% FBS in BD Falcon™ 24-well Multiwell Plate. When cell confluency reached ~30%, the culture medium was replaced with serum-free DMEM, and the plates were returned to the 37 °C incubator. After 2 days, the serum-free medium was removed, and fresh DMEM medium containing 10% FBS, HDL, apoA-II, or lipids from HDL was added. The cells were allowed to grow for 6 h. Cellular proliferation activity was visualized by anti-Histone H3 pS10 antibody staining.

RESULTS

Spatiotemporal Expression of apoa2 during Zebrafish Embryogenesis—To address apoA-II function in embryonic development, we cloned *apoa2* cDNA from zebrafish embryos and found that *apoa2* was highly conserved with other fish (data not shown). To analyze the spatiotemporal expression of *apoa2* in detail during embryonic development, *in situ*, hybridization was performed from the 4-cell stage to 48 hpf embryos using an antisense RNA probe (Fig. 1, *A–K*). *Apoa2* mRNA of maternal origin was detected at the 4-cell stage (Fig. 1*A*), and *apoa2* zygotic transcripts mainly accumulated in YSL (Fig. 1, *C–E*). During epiboly, the *apoa2* transcripts were present in the ventral side (Fig. 1, *D* and *F*). The expression pattern of *apoa2* is similar to *apoa1* and *apoE*, which is associated with lipoprotein synthesis and secretion (9). During the hatching period, *apoa2* exclusively showed high levels in YSL (Fig. 1, *J* and *K*). RT-PCR confirmed the temporal expression pattern of *apoa2* (Fig. 1*L*) in zebrafish embryos. *Apoa2* mRNA was maternal loaded and showed increased levels with the progression of embryonic development after the shield stage, suggesting that zygotic transcription of *apoa2* is initiated at shield stage.

Apoa2 Is Crucial for Epiboly—To examine the function of *apoa2* during zebrafish development, we used two different antisense morpholino oligonucleotides complementary to the translational initiation site of zebrafish *apoa2* mRNA, *apoa2* MO1 and *apoa2* MO2, to knockdown its function in zebrafish embryos. The morpholino oligonucleotides efficiently blocked the expression of zebrafish *apoa2*-green fluorescent protein (GFP)-fused protein in zebrafish embryos (supplemental Fig. S2), suggesting they were able to inhibit the production of endogenous apoA-II protein in zebrafish embryos.

Injection of control MO (*ctl* MO), *apoa2* MO1, MO2, or co-injection with MO1 and MO2 into embryos at the 1-cell stage was performed. Through real-time observation, we found that embryos injected with *apoa2* MO1 or *apoa2* MO2 at the 1-cell stage showed similar developmental defects at the gastru-

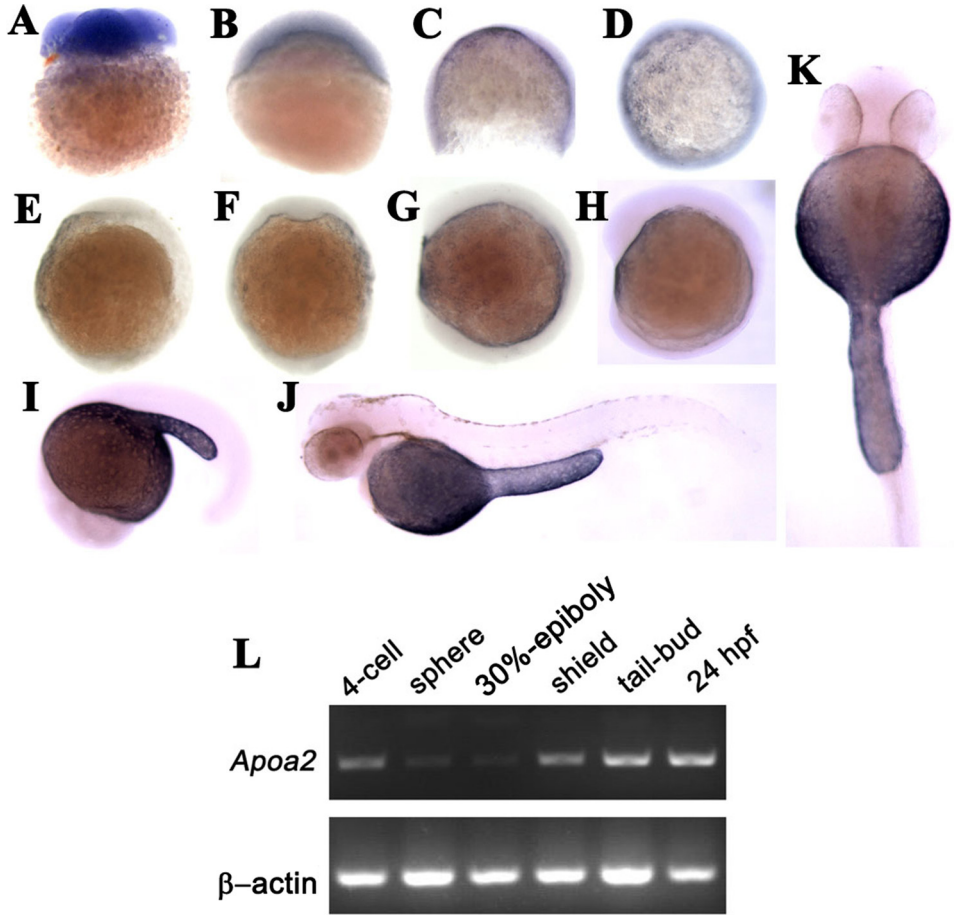

FIGURE 1. Expression pattern of *apoa2* during embryonic and larval development of zebrafish by *in situ* hybridization at 4-cell stage (*A*), 30%-epiboly (*B*), 75%-epiboly (*C*, *D*), tail-bud (*E*, *F*), 4-somite (*G*), 10-somite (*H*), 20-somite (*I*), 48 hpf (*J*, *K*) stages. *L*, RT-PCR detection of *apoa2* expression during embryogenesis at 4-cell, sphere, 30% epiboly, shield, tail-bud, 24 hpf developmental stages. RT-PCR of β-actin expression was used as the RNA-loading control.

lation stage. Embryos injected with *apoa2* MO appeared similar to uninjected embryos or embryos injected with a standard *ctl* MO until the 30% epiboly stage (4.6 hpf). After that stage, the blastoderm and blastoderm margin in the majority of *apoa2* MO-injected embryos became irregular compared with control embryos (Fig. 2, *A*–*D*). In almost half of the defective embryos, it was difficult to identify the formation of the shield, and thus, the dorsal-ventral orientation of the embryo. The embryos failed to progress through epiboly and were lethal because of the great contractile force of the blastoderm margin (Fig. 2, *A*, *C*, and *D*). In many of the *apoa2* MO-treated embryos, the aforesaid defects did not induce death of embryos, and such defects were defined as the "survival" phenotype. The survival embryos injected with *apoa2* MOs were able to develop further and displayed embryonic defects. Many embryos were mildly defective, underwent epiboly, and showed a longer animal-vegetal (AV) axis than control (Fig. 2*H*). The rest of the embryos were severely defective, did not completely cover the yolk cell by the end of the gastrula period, and showed a mildly longer AV axis (Fig. 2*I*).

We were able to reliably rescue *apoa2* morphants by co-injection of capped mRNA of zebrafish *apoa2* that did not contain the MO binding sites or purified native human HDL (purity>95%, contains 0.8 mg/ml apoA-II) (Fig. 2, *E* and *F*). Most rescued embryos survived to 24 hpf, and only a small fraction of embryos underwent yolk lysis. However, some rescued embryos demonstrated various developmental abnormalities (data not shown). Injection of *apoa2*-capped RNA or HDL alone resulted in identical abnormalities, suggesting these are the result of ectopic *apoa2* overexpression rather than partial rescue. Taken together, these results demonstrate that *apoa2* MOs can specifically hinder the activity of endogenous *apoa2* resulting in specific phenotypes.

Apoa2 is specifically expressed in the YSL. We tested whether knockdown of *apoa2* exclusively in the YSL was sufficient to result in epiboly failure by co-injecting *apoa2* or *ctl* MO with rhodamine dextran (RD) into the yolk cell at the 1k-cell stage. Embryos whose blastoderm did not contain RD were scored for phenotype analysis. Epiboly defects were consistently observed in embryos in which RD was restricted to the yolk (Fig. 2, *D* and *J*), and less than 50% of such embryos survived to 24 hpf. Thus, loss of *apoa2* within the yolk cell is sufficient to block epiboly. These results suggest that the normal expression of *apoa2* in YSL is required for embryonic development.

Apoa2 Is Required for Cell Convergence during Gastrulation and Is Not Essential to Dorsoventral Patterning—Most of the survival embryos with the knockdown of *apoa2* function could epiboly, but the movement was delayed or failed to cover the yolk cell at the end of gastrulation; thus we were concerned

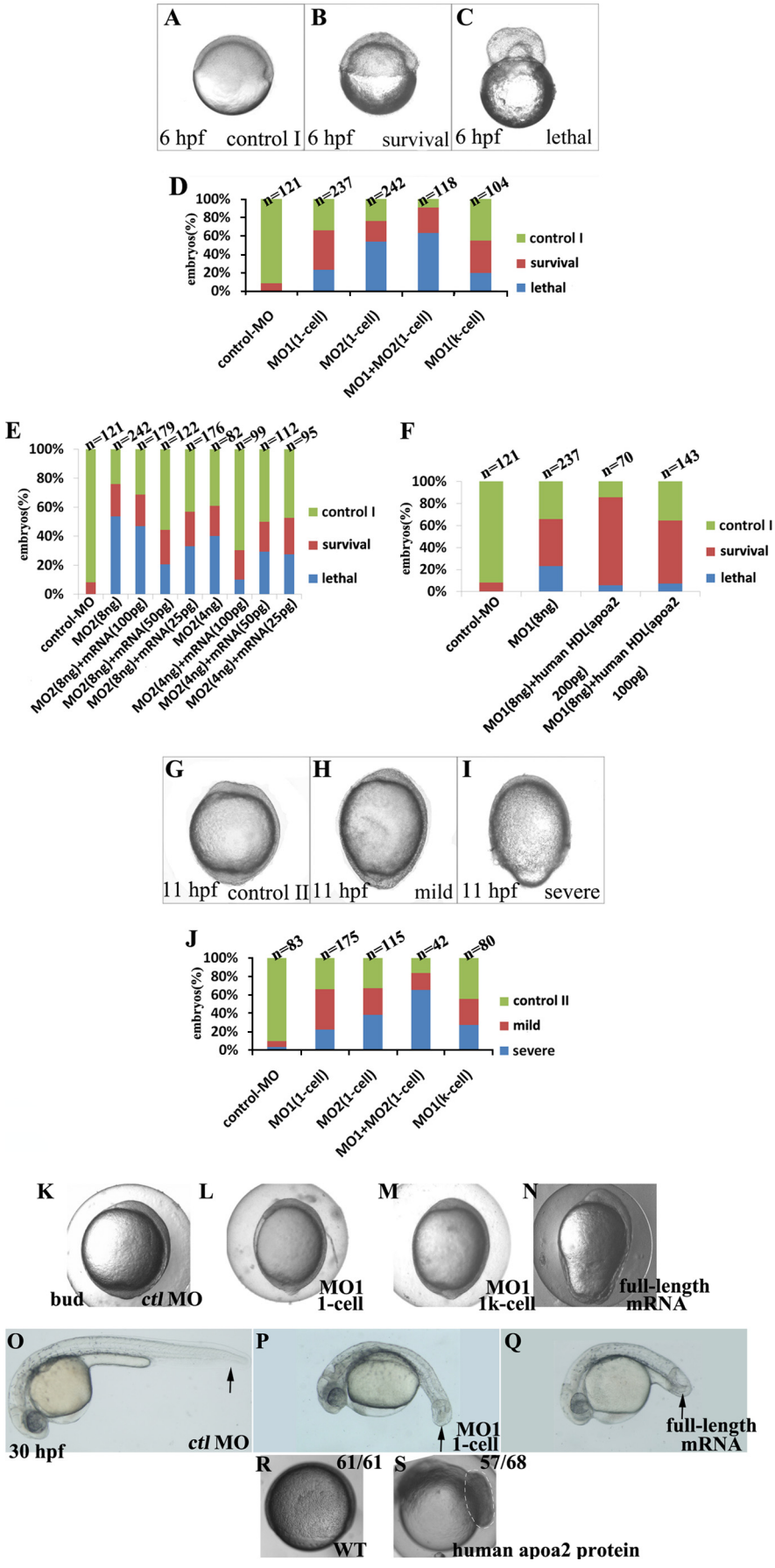
A
6 hpf control I
B
6 hpf survival
C
6 hpf lethal
D
embryos(%)
100%
80%
60%
40%
20%
0%
n=121
n=237
n=242
n=118
n=104
control I
survival
lethal
control-MO
MO1(1-cell)
MO2(1-cell)
MO1+MO2(1-cell)
MO1(k-cell)
E
n=121
n=242
n=179
n=122
n=176
n=82
n=99
n=112
n=95
control-MO
MO2(8ng)
MO2(8ng)+mRNA(100pg)
MO2(8ng)+mRNA(50pg)
MO2(8ng)+mRNA(25pg)
MO2(4ng)
MO2(4ng)+mRNA(100pg)
MO2(4ng)+mRNA(50pg)
MO2(4ng)+mRNA(25pg)
F
n=121
n=237
n=70
n=143
control-MO
MO1(8ng)
MO1(8ng)+human HDL(apoa2 200pg)
MO1(8ng)+human HDL(apoa2 100pg)
G
11 hpf control II
H
11 hpf mild
I
11 hpf severe
J
n=83
n=175
n=115
n=42
n=80
control II
mild
severe
K
bud
ctl MO
L
MO1 1-cell
M
MO1 1k-cell
N
full-length mRNA
O
30 hpf
ctl MO
P
MO1 1-cell
Q
full-length mRNA
R
61/61
WT
S
57/68
human apoa2 protein

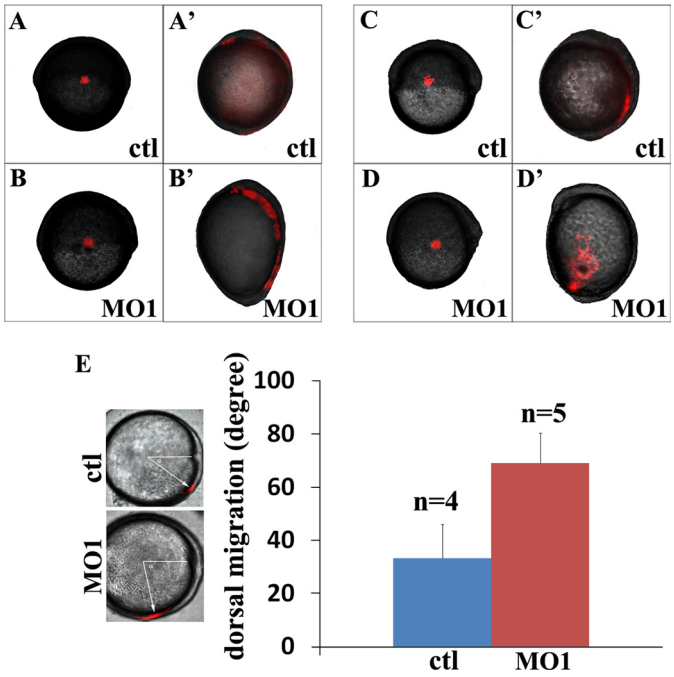

FIGURE 3. ***Apoa2* regulates convergence of lateral cells.** Labeled lateral mesendermal cells at shield stage in 8 ng *ctl* MO (*A*, *C*) or *apoa2* MO1 (*B*, *D*) injected embryos were observed and imaged at the tail-bud stage (*A′*, *B′*, *C′*, *D′*, respectively). (*A′–B′*, *C–D*, and *C′–D′*) show lateral views and (*A–B*) show dorsal views. *E*, quantification of dorsal migration of lateral cells.

about whether there were defects in cell movement during embryonic morphogenesis. We used a Kaede-mediated photoconversion strategy to test the ability of anterior migration of axial cells and dorsal convergence of lateral cells, respectively. Dorsal migration of lateral cells in *apoa2* MO1-injected embryos was reduced (Fig. 3, *C–D′* and *E*), and anterior movement of axial cells showed no significant difference compared with *ctrl* MO embryos (Fig. 3, *A–B′*). Then the embryos which displayed "mild" phenotype as described (Fig. 2*H*) were examined by the expression of marker genes in embryos with knockdown *apoa2* by whole-mount *in situ* hybridization (supplemental Fig. S2, *A–N*). *apoa2* MO embryos exhibited longer notochord marked with *no tail* (*ntl*), slightly wider neural plate marked with *distal-less homeobox gene 3* (*dlx3*), and normal position of prechordal plate assessed by hatching gland 1 (*hgg1*), in comparison to control embryos (supplemental Fig. S2, *A–F*). Alteration of the expression pattern of *dlx3* revealed that inhibition of *apoa2* expression induced reduction for convergence of neuroectoderm. Myogenic differentiation 1 (*myoD*) and paraxial protocadherin (*papc*) expression in paraxial and lateral mesoderm appeared to be mediolaterally expanded in the embryos lacking *apoa2* (supplemental Fig. S2, *G–J*). The altered expression of forkhead box D3 (*foxD3*) indicated that convergence of neural crest was interfered in embryos with loss of *apoa2* (supplemental Fig. S2, *K* and *L*). The paraxial distribution of SRY-box containing gene 17 (*sox17*) labeling progenitors of endoderm cells were disturbed with injection to *apoa2* MO1 embryos (supplemental Fig. S2*N*) compared with control embryos (supplemental Fig. S2*M*), suggesting that the normal movement of endodermal cells was impaired with knockdown of *apoa2*. Together, the results indicate that *apoa2* affected cell convergence movement during the gastrula period.

Convergence and extension are key steps for dorsoventral (DV) patterning during embryonic gastrulation (21). Therefore, to determine whether *apoa2* also functioned in DV patterning, we examined the expression of a variety of DV marker genes in embryos, which were injected with *apoa2* MO1 at the 1-cell stage and exhibited the "survival" phenotype (Fig. 2*B*), by whole-mount *in situ* hybridization (supplemental Fig. S2, *O–V*). In *apoa2* MO embryos, the expression of floating head (*flh*) and goosecoid (*gsc*) displayed no significant changes (supplemental Fig. S2, *O–R*). The expression of *GATA-binding protein 2* (*gata2*) and *even-skipped-like 1* (*eve1*) was also not visibly altered (supplemental Fig. S2, *S–V*). These results show that impairment of endogenous *apoa2* mRNA activity does not apparently affect the dorsoventral differentiation.

Mtx2 Expression and the F-actin Ring in YSL Are Altered in apoa2 Morphants—The proper organization of YSL has been shown to be essential for initiation and progression of epiboly in teleosts (21, 31). *Apoa2* is dominantly expressed in the YSL and performs a function in zebrafish embryonic gastrulation. Therefore, the expression of the YSL-specific gene *mtx2* (21, 31) was examined to determine whether the function of YSL had been altered in knockdown *apoa2* embryos. These results showed that loss of *apoa2* decreased *mtx2* expression significantly in the blastoderm margin (70%, $n = 20$, Fig. 4, *A* and *B*).

The disorganization of eYSL may also perturb the F-actin band of the eYSL (32). A punctate band of filamentous actin (F-actin) has been described at the periphery of the eYSL and the EVL margin from 50% epiboly onwards (32, 33). Therefore, we used anti-F-actin antibody to stain microfilament structures in the yolk. At shield stage, the punctate F-actin ring was visible below the blastoderm margin in *ctl* MO-injected embryos (Fig. 4, *C* and *F*). The F-actin ring was either weakly formed, or failed to form at all, in *apoa2* MO-injected embryos (Fig. 4, *I* to *L*). In contrast, other actin-based structures were still visible in *apoa2* MO-injected embryos. Thus, the actin is expressed in the absence of *apoa2* but is disorganized specifically in the eYSL. This suggests that *apoa2* may be required in the eYSL for polymerization of actin rather than actin expression *per se*. Taken together, the results of the alteration of *mtx2* expression and actin band formation in *apoa2* MO-injected embryos suggest *apoa2* is required for YSL organization that properly drives embryonic epiboly.

The YSL Is Disorganized in apoa2 Morphants—Next, we examined the YSL structures in *apoa2* MO-injected embryos.

FIGURE 2. **Inhibition *apoa2* function at 1-cell or 1k-cell stage induced defective epiboly.** *A–C*, *G–I*, phenotypes of loss of *apoa2* function at 6 hpf (*A–C*) and 11 hpf (*G–I*) embryo, lateral view. (*D*, *J*): range of phenotypes during gastrulation is induced by injection with *apoa2* MO1 or *apoa2* MO2 at 1-cell or 1k-cell stage as indicated. *E* and *F*, quantification of phenotypes are produced by *apoa2* MO morphants, with or without *apoa2* mRNA or human HDL. Overexpression or knockdown *apoa2* (injection of MOs was performed at 1-cell or 1k-cell stage) led to the body axis elongated during late gastrula, and short posterior trunk and curved tail at 30 hpf (*black-arrow* indicates the tail) (*K–Q*). Embryos were injected with 180 pg of apoA-II protein at the 1-cell stage and imaged at 75%-epiboly stage. The *dashed region* indicates excessive cell proliferation (*R*, *S*).

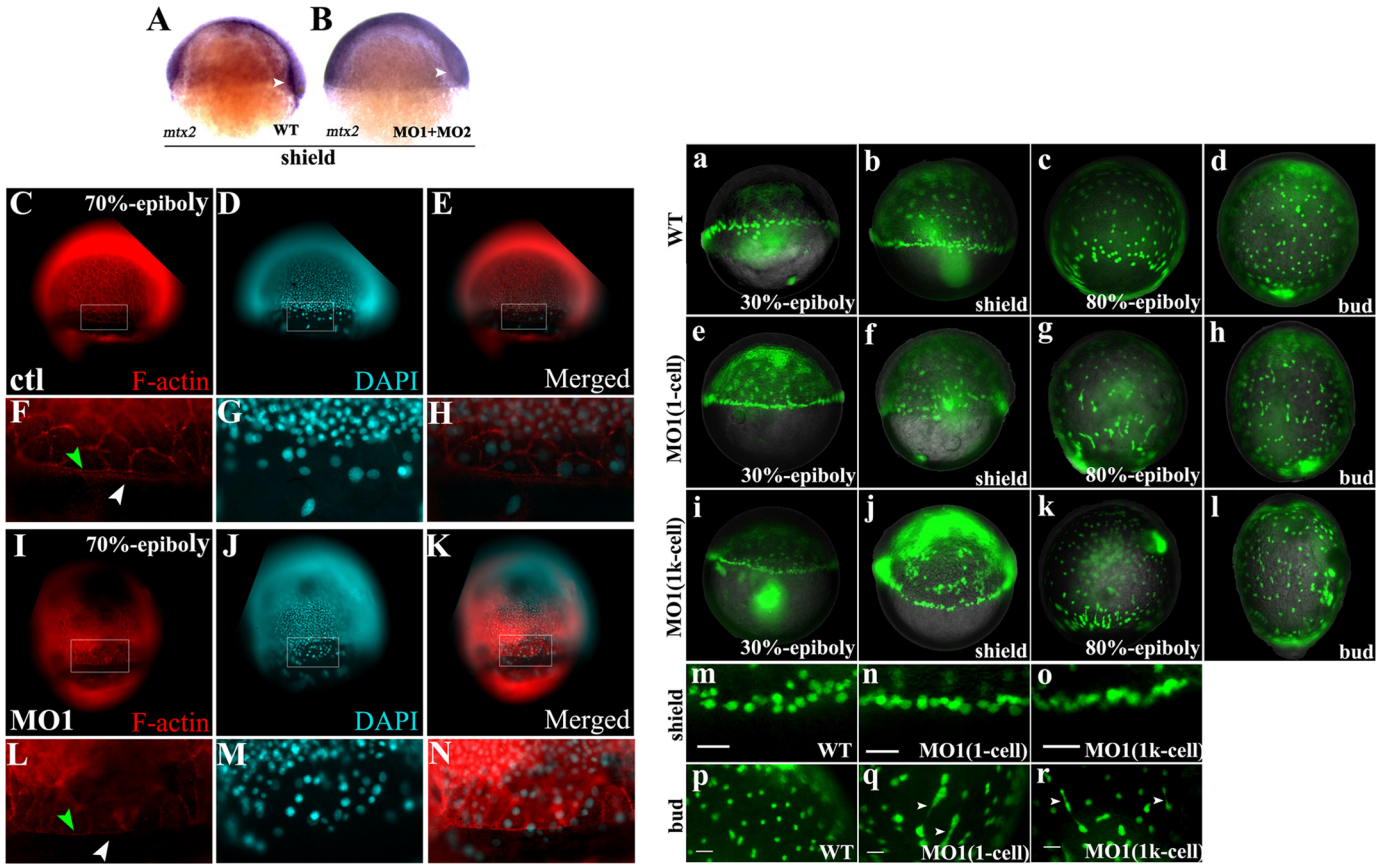

FIGURE 4. ***mtx2* expression and the F-actin ring are altered in *apoa2* morphants and YSN are disordered in the absence of *apoa2* function.** *A*, *mtx2* expressed as YSL-specific gene expressed blastoderm margin at shield stage. *B*, *mtx2* expression was decreased significantly with loss of *apoa2*. *White arrowheads* indicate the blastoderm. *C–N*, F-actin antibody and DAPI-stained embryos pre-injection with *ctl* MO or *apoa2* MO1 at the 1-cell stage. *F–H* and *L–N* denotes magnified views of the regions marked by *rectangles* in *C–E* and *I–K*. The F-actin punctate band of the eYSL (indicated with *white arrowhead*) and the peripheral F-actin ring within the EVL (indicated with *green arrowhead*) are shown. Wild-type (*a–d* and *m*, *p*) and *apoa2* MO1 (injection at 1-cell) (*e–h* and *n*, *q*), *apoa2* MO1 (injection at 1k-cell) (*i–l* and *o*, *r*) embryos were injected with SYTOX Green at the 1k-cell stage, then observed and imaged at 30%-epiboly, shield, 80%-epiboly, and tail-bud stages. The YSN at blastoderm margin exhibited abnormal aggregation in the *apoa2* losing embryos (*n* and *q*) compared with wild-type (*m*) at the shield stage. YSN were regularly spaced in wild-type (*p*); but random distribution in *apoa2* MO1 (*q* and *r*). The *white arrowhead* indicates incomplete dissociation of YSN. Scale bar, 50 μm. (*b–c*, *f–g*, and *j–k*) show lateral views and (*d*, *h*, and *l*) show dorsal views.

During blastulation, gastrulation, and early segmentation, zebrafish YSN display several highly patterned movements to organize YSL (18). We injected the vital dye SYTOX Green into the YSL at the 512-cell and 1k-cell stages to inspect the spatial organization of YSN as described previously (21). The YSN within the ring at the blastoderm margin appeared abnormal in distribution and morphology in embryos injected with *apoa2* MO (Fig. 4, *a–r* and supplemental Fig. S3). The YSNs within the ring at the blastoderm margin appeared abnormally dense (Fig. 4, *a–b*, *e–f*, and *m–n*) and the YSNs under the blastoderm were not properly dispersed (Fig. 4, *c–d*, *g–h*, and *p–q*) in embryos injected with *apoa2* MO1 at the 1-cell stage. Many of the YSNs displayed irregular shapes. Some nuclei connected together by DNA context and the others showed variable rod shapes in the *apoa2* MO1 embryos (Fig. 4*q*). Co-injection with *apoa2* MO1 and SYTOX Green into yolk at the 1k-cell was also performed. These results showed that the YSNs showed similar defects (Fig. 4, *i*, *j*, *k* and *l*). Irregular YSNs were consistently observed until late gastrulation (Fig. 4*r*). During early epiboly, abundant YSNs were accumulated at the blastoderm margin in the absence of *apoa2* (Fig. 4, *m–o*, supplemental Fig. S3, *A–A′*, *B–B′*, *D–D′* and *E–E′*). DAPI staining also displayed the irregular nuclei in YSL (supplemental Fig. S3, *F–K′*). When the YSNs were normal shape, they were able to continue epiboly (supplemental Fig. S3, *C–C′* and *K–K′*) in *apoa2* MO-injected YSL.

We measured the distance among the YSNs of wild-type embryos and *apoa2* MO embryos. YSNs from wild-type embryos were significantly dispersed at greater than about 10 μm length scales, with a maximum incidence at around 22 μm as previously mentioned (21). The spatial organization of YSNs was seen in *apoa2* MO embryos on length-scales smaller than 6 μm and showed aggregation in some regions within eYSL and iYSL (Fig. 4, *a–r* and supplemental Fig. S3). In such regions, most of the nuclei were irregular in shape and bigger in size. In other regions of YSL, this spatial organization of YSNs was dispersed at greater than 30-μm length-scales. YSN distributed sporadically in such regions in the YSL cytoplasm. These results indicate that the external and internal YSNs were not properly dispersed and appeared to have lost their spatial constraints in *apoa2* MO embryos. We also calculated the spatial distributions of YSN using Ripley's K-function as described (21, 34) and obtained a similar conclusion (data not shown). Taken together, the data show here that abnormal and aggregated

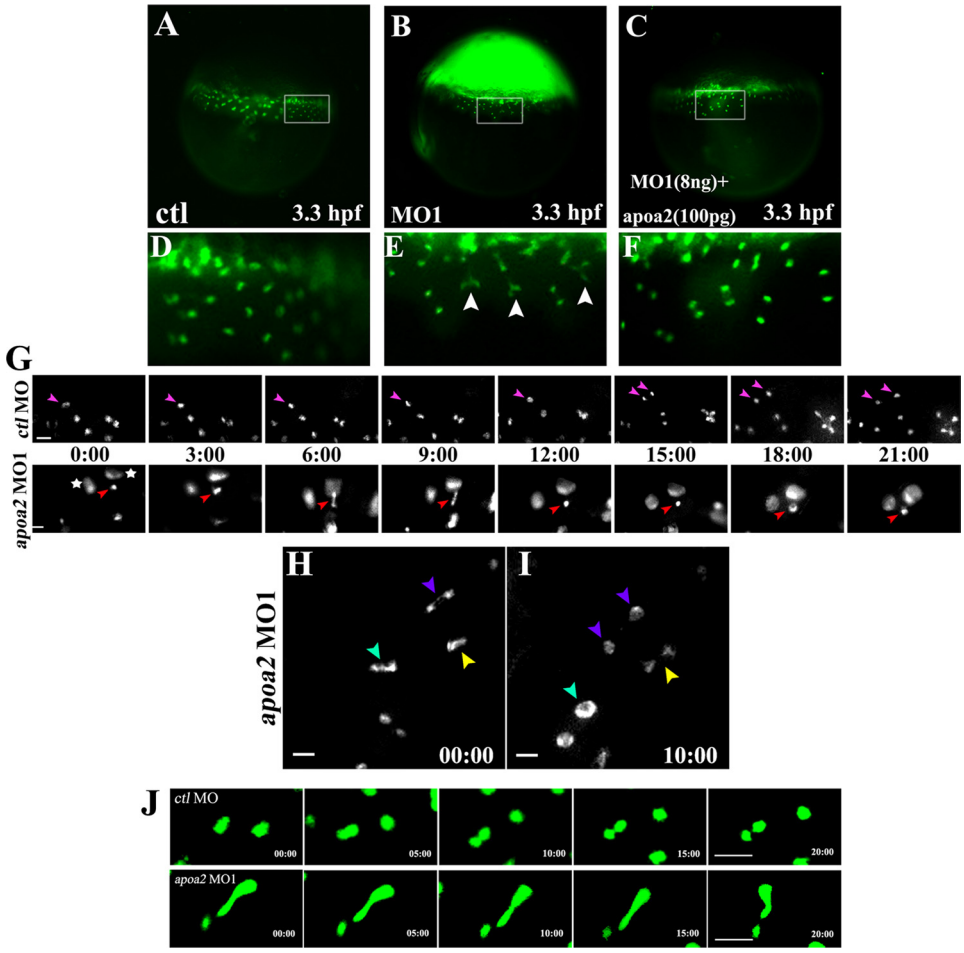

FIGURE 5. **Time-lapse imaging of the YSN division in *apoa2* MO embryos.** Injection with 8 ng of control MO or *apoa2* MO1 or co-injection with 8 ng of *apoa2* MO1 with human HDL (contains 100 pg of Apoa II) was performed at the 1-cell stage. At the 512-cell stage, SYTOX Green was injected. Images of embryos were taken at the 1k-cell-sphere stage (*A–I*). *D–F* denotes magnified views of the regions marked by *rectangles* in *panels A–C*. The YSN (labeled with SYTOX Green) showed severely defective nuclear division (indicated with *white arrowhead*) in *apoa2* MO1-injected embryos ($n = 31$) (*E*) but did not emerge the phenotype in *apoa2* MO1 and human HDL-co-injected embryos ($n = 10$) (*F*) compared with control embryos ($n = 8$) (*D*). *G*, progression of complete and incomplete division of the YSN were captured in the control embryo and *apoa2* MO1-injected embryo, respectively. The *pink arrow* indicates the normal dividing nucleus, and the *red arrow* indicates defective nuclear division. Images were taken every 3 min. The aggregated nuclei are indicated by an *asterisk*. *H*, *I*, real time tracing of three incompletely divided nuclei are shown in the *apoa2* MO1-injected embryo. A severe defect in nuclear division is indicated with the *cyan arrowhead*, and medial and slight defects are indicated with *purple* and *yellow arrowheads*, respectively. *H* and *I* were intervals of 10 min. Scale bar, 20 μm. *J*, examples of real time tracing show YSN movements during the progression of YSL patterning. *Upper panel*: two nuclei moved apart, away from each other to disperse in the cytoplasm of YSL in *ctl* MO embryos. *Lower panel*: the two connected nuclei in *apoa2* MO embryo underwent back and forth movement during the progression of YSL patterning. Scale bar, 50 μm.

nuclei cause the spatial disorganization of YSN in *apoa2* morphants.

Apoa2 Controls the Division of YSL Nuclei—We find that the YSNs are in an irregular shape after disruption of *apoa2* expression. Therefore, we started to monitor how the irregular nuclei formed during the YSL formation by real time tracing of YSL formation and patterning (Fig. 5). YSL formation usually began after the 512-cell stage as described (16). The blastomeres at the boundary with the yolk cell collapsed to release their nuclei into yolk cell to form YSL. The cellular nuclei in blastomeres at the boundary had a normal shape and were perfectly divided. When the YSN appeared in YSL, they started their first division (16) (Fig. 5, *A* and *D*). The YSN divided smoothly and completely separated to form two daughter nuclei in wild-type YSL. In the *apoa2* MO1 embryos, the first YSNs appeared as a normal shape and then began to divide. However, the division of the YSN was incomplete, and the dividing YSN were unable to separate from each other (Fig. 5, *B*, *E*, *G*, *H*, *I*, and supplemental Fig. S4). Injection of the human HDL was able to rescue the defects of YSN division (Fig. 5, *C* and *F*). We had continually traced the YSN division and found that disruption of *apoa2* caused incomplete YSN division until the last YSN division during the progression of YSL formation (Fig. 5*G*). These results indicate that *apoa2* is required for the proper division of the YSN.

The Defective Divided Nuclei Cause Disordered YSN Movements—During real time tracing, we observed that when the YSN division ceased, YSL began to move for patterning as in previous observations (16). YSN in *ctl* MO embryos moved apart from each other in eYSL and iYSL for YSL epiboly and convergence and extension movements (Fig. 5*J*). However, the incompletely divided YSN in *apoa2* MO embryos were pulled to form rod-shaped nuclei by the force from movements of YSL cytoplasm (Fig. 5*J*). When the two incompletely divided nuclei extended some distance, the nuclei were drawn back. The back

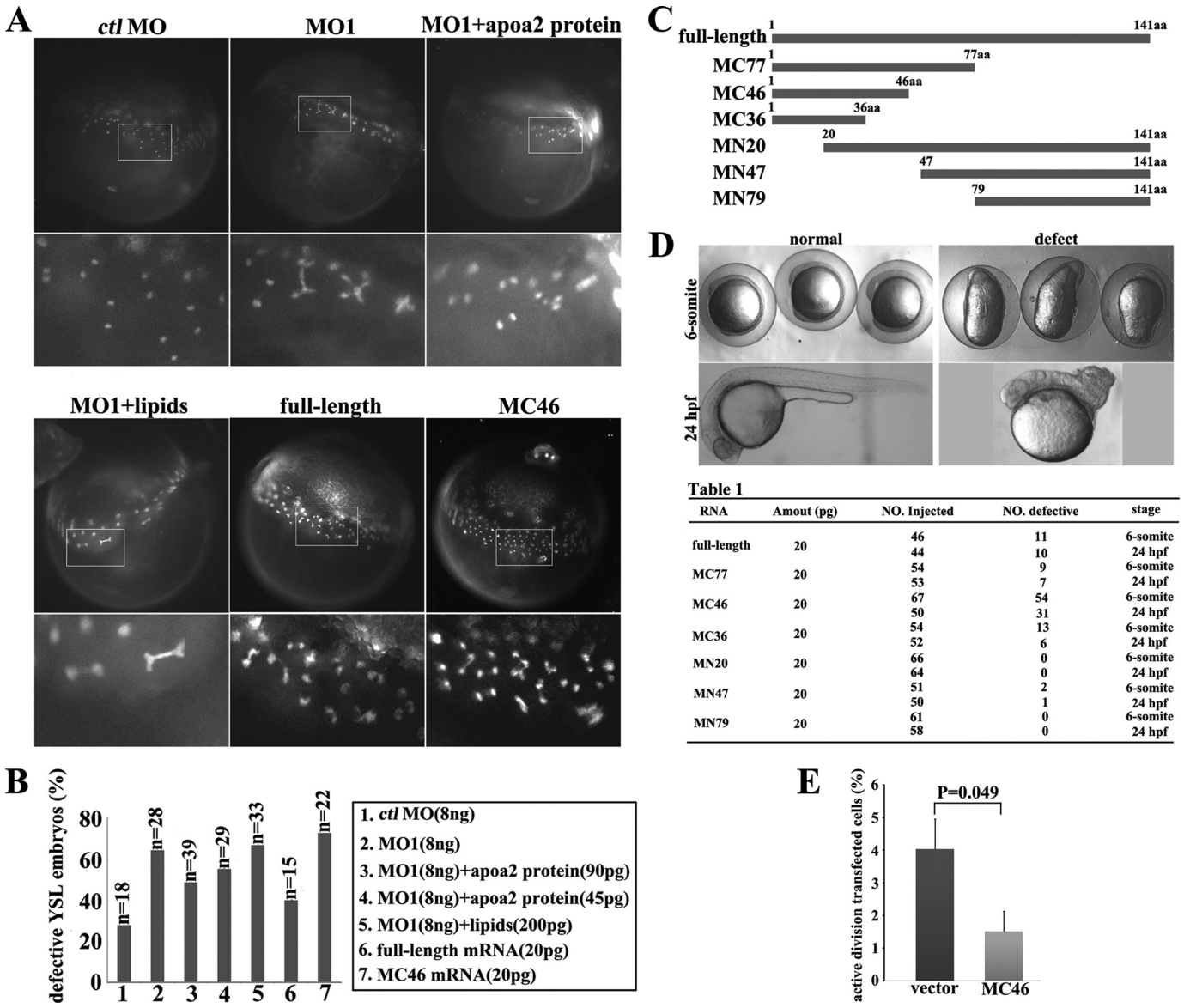

Table 1

RNA	Amout (pg)	NO. Injected	NO. defective	stage
full-length	20	46	11	6-somite
		44	10	24 hpf
MC77	20	54	9	6-somite
		53	7	24 hpf
MC46	20	67	54	6-somite
		50	31	24 hpf
MC36	20	54	13	6-somite
		52	6	24 hpf
MN20	20	66	0	6-somite
		64	0	24 hpf
MN47	20	51	2	6-somite
		50	1	24 hpf
MN79	20	61	0	6-somite
		58	0	24 hpf

FIGURE 6. **The apoA-II protein is required for YSN division.** *A*, injection of 8 ng of *ctl* MO, 8 ng of a*poa2* MO1, 8 ng of a*poa2* MO1 plus 90 pg of apoA-II protein, 8 ng of *apoa2* MO1 plus 1 ng of lipids, 20 pg of *apoa2* full-length mRNA, or 20 pg of *apoa2* C-terminal mutant MC46 mRNA into yolk was performed at the 512-cell stage, and the SYTOX Green was injected into yolk at the 1k-cell stage. The *lower panel* denotes magnified views of the regions marked with *white boxes* in the *upper panel*. *B*, quantification of the phenotypes derived from human apoA-II protein, lipids, overexpression zebrafish *apoa2* full-length mRNA, or *apoa2* C-terminal mutant MC46 mRNA as indicated. The constitution of the apoa2 mutations is shown (*C*). *D*, injection with the mutations mRNA at the 1-cell stage induced severe elongation of body axis at the 6-somite stage and dorsalization at 24 hpf. Detailed statistics of the phenotype caused by various apoa2 mutations (table) are shown. *E*, quantification of the mitotic activity in the transfected human HeLa cells is shown.

and forth movements of the defective nuclei were observed during the progression of YSL patterning and blocked the proper organization of YSL. Finally, irregular YSL patterning caused defects in embryonic gastrulation. Taken together, these results indicate that the normal division and patterning of YSNs play an essential role in embryonic cell movements.

ApoA-II Protein Modulates Chromosome Separation during Nuclear Division in Zebrafish Embryos and in Human Cells—As the HDL was able to ease the defect of nuclear division in YSL of zebrafish embryos, we tried to examine which components in the HDL perform the function. HDL consists of proteins that include apoA-II and lipid. We purified the apoA-II and total lipid from human HDL. Then, injection with the combination of MO1 and the apoA-II protein or lipid into the embryo yolk at 512-cell stage was performed. Noticeably, the apoA-II protein, not the lipid, was able to rescue the YSL defects because of loss of function of *apoa2* in zebrafish embryos (Fig. 6, *A* and *B*). In addition, the abnormal proliferation of embryonic cells was noted at the 75%-epiboly stage (Fig. 2, *R* and *S*) when the embryos were subjected with apoA-II protein only. To further clarify the function of apoA-II on nuclear division, six mutants of *apoa2* were generated (Fig. 6*C*). The *apoa2* C-terminal deletion mutant MC46, which was missing 95 amino acids from the C terminus and retained the signal peptide of the N terminus, was able to induce strongly YSN defective division similar to MO phenotypes and cause severe embryonic defects (Fig. 6*D*, *table*). The mutant did not affect the formation of mitotic spindles (supplemental Fig. S6). These

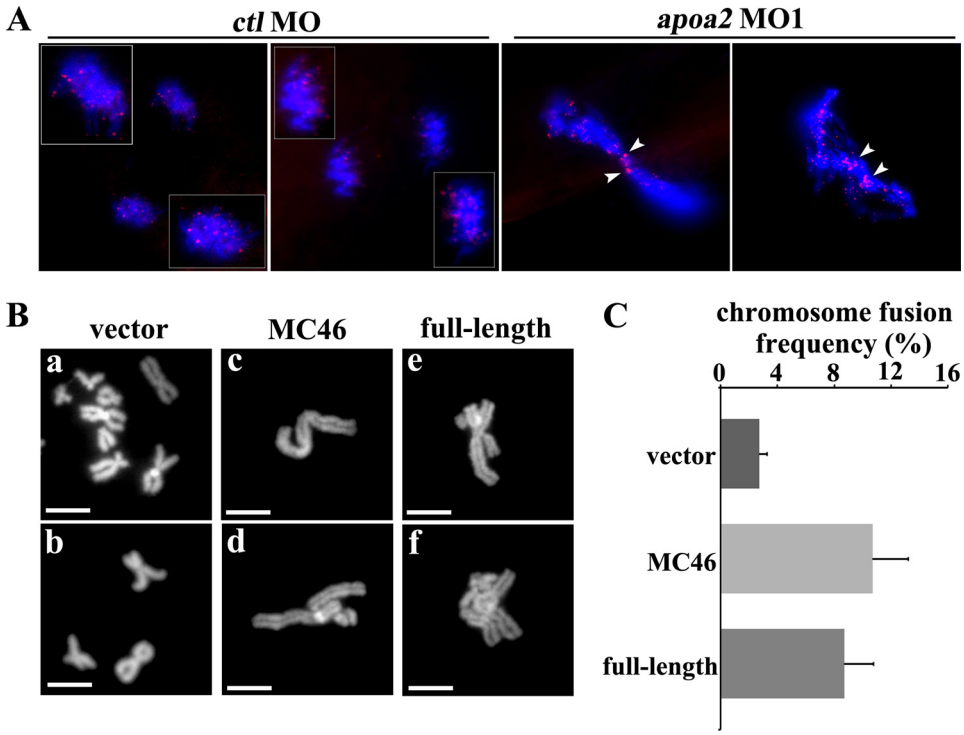

FIGURE 7. **Alteration of the *apoa2* function induces chromosomes fusion.** *A*, 8 ng of *ctl* MO or *apoa2* MO1 were injected at the 1-cell stage, and the telomeres in YSN were detected using FISH (fluorescence *in situ* hybridization) with Cy3-labeled (GGGTTA) 7 oligomers and DAPI-counterstain at the sphere stage. *White arrowheads* indicate the abnormal accumulation of telomeres. *B*, exhibition of the morphology of metaphase chromosomes in HeLa cells after overexpressing GFP, full-length *apoa2*-GFP, and GFP-fused *apoa2* C-terminal mutant MC46. Metaphase chromosomes separated mutually (*a*– *b*) in control and fused morbidly (*c*–*f*) in the case of loss or gain of the function of apoA-II protein. Scale bar, 50 μm. *C*, quantification of the chromosome fusing frequency in transfected human HeLa cells is shown.

results suggest that the C-terminal peptide is required for nuclear division and indicate that the mutants hindered the function of endogenous apoA-II protein, suggesting that apoA-II indeed plays an essential role in nuclear division in YSL.

We discovered that the DNA content connected during nuclear division in YSL after disruption of apoA-II function; therefore, we tested which factor caused defective nuclear division in YSL. The telomeres of chromosomes were detected in dividing YSN. These results confirmed that loss of the *apoa2* function induced DNA context to be unable to separate during the YSN division. The abnormal aggregation of telomeres was also detected in the dividing YSN, suggesting that the chromosomes may be fused during the progression of nuclear division in YSN (Fig. 7*A*). However, we failed to isolate and examine the detailed structures of the chromosomes from YSN because of the large number of embryonic cells.

For alteration, we overexpressed and found GFP-fused *apoa2* C-terminal mutant MC46 inhibited cell growth in the human HeLa cell line (Fig. 6*E*, supplemental Fig. S5*B*). Then, we wanted to know whether apoA-II had an impact on the activity of cell division in human cells. HeLa cells were first cultured with serum-free medium in 24-well plates for 48 h to reduce cell proliferation (supplemental Fig. S5*A*). Then, serum, human HDL, apoA-II protein, or HDL lipid was subjected to cells. 6 h later, the multiplicative activities of HeLa cells were monitored. These results showed that the HDL and apoA-II protein were able to stimulate the division of HeLa cells effectively (supplemental Fig. S5, *A* and *B*). In contrast, lipids were hardly effective in stimulating cell division, indicating that apoA-II protein also modulates cell growth in human cells. The metaphase chromosomes of HeLa cells during mitotic phase were examined. These results showed that the many chromosomes were fused to each other in cells with overexpression of the *apoa2* C-terminal mutant (Fig. 7, *B* and *C*). In addition, the overexpression of full-length *apoa2* also caused chromosome fusion (Fig. 7, *B* and *C*). These results were consistent with above observations that *apoa2* overexpression induced defective YSN division in zebrafish embryos. Taken together, the data obtained from human cells and zebrafish embryos indicate that the function of apoA-II prevents chromosome fusion during nuclear division and is conserved in zebrafish cells and in human cells.

DISCUSSION

In this study, we provide a novel function for apolipoprotein *apoa2* during zebrafish embryogenesis. A*poa2* is dominantly expressing in YSL. Knockdown of *apoa2* mRNA translation reveals that *apoa2* prevents chromosome fusion to control YSN division and organization to regulate cellular movements during zebrafish embryonic development. Our results suggest that proper YSN division and distribution provide the sufficient hardness and tension in the big yolk cell to meet the requirements of the embryonic cell moving during embryonic development, consistent with the fact that the factors in the YSL are able to modulate embryonic cell movements (35, 36). In addition, apoA-II also prevents chromosome fusion during nuclear division in human cells, suggesting the function of apoA-II in nuclear division is conserved in animal cells.

A Specific Gene Expression in YSL Is Able to Modulate Embryonic Development—Several early developmental genes, including *sqt*, *cas*, and *gata5*, are expressed both in the YSL and adjacent vegetal blastomeres (25). Disruption of these genes causes the YSL disorganization and induces embryonic defects. However, these genes could not provide clear evidence that YSL formation is crucial for embryonic development, because these genes also play essential roles in embryonic patterning. Injections of RNase into the YSL that RNase effectively eliminates YSL transcripts without affecting ubiquitously expressed genes in the blastoderm demonstrate that RNA in the YSL is required for the formation of ventrolateral mesendoderm and induction of the nodal-related genes in the ventrolateral marginal blastomeres (38). Previous works have also shown that some genes regulating YSL morphogenetic movements including e-cadherin and *Mtx2* (21) are able to modulate embryonic development. Now, we provide more evidence to show that impairment of *apoa2* in YSL is able to disrupt YSN division and organization, resulting in the defects of embryonic development in zebrafish. Our work on the function of zebrafish *apoa2* in the YSL directly illustrates that the YSL organization affected by a gene expressed in the YSL, restrictively, plays an essential role during embryonic development.

YSN Division Plays Crucial Roles during Embryogenesis—The YSL provides the major force in the vegetal spreading of the overlaying blastoderm (35). The epiboly begins with eYSL contraction, which causes narrowing of the eYSL and crowding of its nuclei to expend both nuclei and cytoplasm of iYSL and to commence embryonic epiboly (16). Following this initial expansion, the YSL continues its independent expansion toward the vegetal pole. Embryonic gastrulation undergoes correctly along the expansion. Microfilaments forming a concentric ring in eYSL are proposed to generate a constrictive force that would drive expansion of the YSL (16, 39). We find that disruption of *apoa2* function induced the disordered microfilament arrays in the YSL. However, previous studies and our observations show that microfilament bundles appear after 50% epiboly (39). In *apoa2*-disrupted embryos, the YSN disorders occur just after the multiple nuclei appear in the yolk cell and induce YSL disorganization, indicating that the disorder of microfilament bundles is the consequence of the YSN disorganization. The microtubules were also identified to contribute to various aspects of epiboly, and that they are primarily involved in movements of the YSN. In the *apoa2*-disrupted embryos, we do not find the disorganization of microtubules (data not shown). Therefore, the driving force in YSL for developmental defects in *apoa2*-disrupted embryos does not come from the cytoskeleton.

At present, it is still unclear whether coordinated convergence movements of the blastoderm and underlying YSN play crucial roles during embryogenesis. On the one hand, cellular and nuclear movements of mesendoderm and YSL are highly coordinated during gastrulation (16, 37) in zebrafish embryos. YSN convergence movements depend on mesendoderm convergence that directs YSN convergence movements (17). On the other hand, transcription in YSN is crucial for mesendoderm cell fate and heart progenitor cell migration (38, 40, 41), suggesting the YSN patterning plays a role for embryonic movements. Our data show that the disruption in YSN division induces defects in YSN movements, resulting in default in embryonic movements. The facts indicate that YSN patterning is essential for embryogenesis and that the YSN convergence movements are indeed required for blastoderm patterning and/or morphogenesis on the normal embryonic epiboly.

In teleosts, YSL forms mainly by collapse of certain marginal blastomeres, which then merge with the cytoplasm of the yolk cell peripheral to the blastoderm (16). Nuclei enter the yolk cell from these open blastomeres most frequently at cleavages 9 and 10 (16). After entry, the first nuclei divide three to five times. After each nuclear division, the YSL increases in width, and its nuclei are quite evenly spaced (16). After the last mitosis, when the YSL is at its widest, YSN initiates long-range convergent extension movements toward the dorsal midline during the mid-gastrula stage (17). There is an extension in the AP direction of the YSN that either reside in, or enter, the dorsal region (38). The initiating force for the YSN movements comes from contraction of eYSL (16). We identify that *apoa2* is required for nucleus division from the cleavages 9 and 10 to the cease of nuclear division in YSL. Blocking *apoa2* expression causes the incomplete divided nucleus. The defective nuclei within eYSL cause the contraction of eYSN disordered, are unable to separate apart and move into the region of iYSL, and block narrowing and expanding the YSL along the AP direction of embryos. Within iYSL region, the uncompleted dividing nuclei also appear aggregated, could not separated, and hinder the YSN movements, resulting in embryonic morphogenetic movement and development failure in embryogenesis. The data clearly demonstrate that the YSN division plays an essential function during the embryonic development.

ApoA II Is Essential for Embryonic Development in Zebrafish—The mature apoA-II protein is the second main constitutive component of HDL, representing ~20% by weight of the HDL protein (42). Data derived from the study of genetically modified mice suggest that apoA-II is essential in all animal species and modulates the structure and biology of HDL and of lipoprotein metabolism in general. Disruption of apoA-II in mice showed a dramatic decrease in plasma HDL cholesterol associated with a rapid clearance of remnant particles, suggesting an important role of apoA-II in triglyceride metabolism (42). Overexpressing apoA-II has elevated plasma levels of triglycerides and free fatty acids in addition to a decrease in triglyceride hydrolysis (43). Furthermore, an increased expression of apoA-II causes an acute inhibitory effect on the hydrolysis of VLDL and chylomicron triglycerides (44). All of these observations indicate that apoA-II play an essential role in lipid metabolism. Now, we show *apoa2* is crucial for YSN division and organization during zebrafish embryonic development. The data suggest that apolipoproteins not only perform functions in lipoprotein formation but also affect the YSN division and YSL formation during embryonic development. We also observe that the apoA-II induces proliferation of the human cell line. C-terminal deletion of apoA-II protein causes the defective nuclear division in YSL of zebrafish embryos and in human cells. These results indicate that apoA-II not only plays an essential role in YSN division, but also acts as a crucial factor in nuclear division of mammalian cells, and that apoA-II in the

regulation of nuclear division is conserved in animal cells. During these experiments, we also examined the structures of microtubule, which play very important roles during nuclear division, and found out there was no alteration of microtubule structure including the formation of mitotic spindles (supplemental Fig. S6) in apoA-II protein-treated cells, These results are consistent with our observations in YSL in zebrafish embryos and indicate that apoA-II could not affect microtubule formation in the cell. The fact that the C terminus but not the signal peptide is required for nuclear division suggests that the apoA-II performs a more complicated function, not just acting as a signaling component in nuclear division. Additional experiments are required to understand in detail how apoA-II prevents chromosome fusion in cells.

REFERENCES

1. Havel, R. J. (1975) *Adv. Exp. Med. Biol.* **63,** 37–59
2. Li, W. H., Tanimura, M., Luo, C. C., Datta, S., and Chan, L. (1988) *J. Lipid Res.* **29,** 245–271
3. Paolucci, M., Guerriero, G., Botte, V., and Ciarcia, G. (1998) *Comp. Biochem. Physiol. B Biochem. Mol. Biol* **119,** 647–654
4. Monnot, M. J., Babin, P. J., Poleo, G., Andre, M., Laforest, L., Ballagny, C., and Akimenko, M. A. (1999) *Dev. Dyn.* **214,** 207–215
5. Lange, P. H. (2005) *Nat. Clin. Pract. Urol.* **2,** 151
6. Kondo, H., Kawazoe, I., Nakaya, M., Kikuchi, K., Aida, K., and Watabe, S. (2001) *Biochim. Biophys Acta* **1531,** 132–142
7. Ando, S., Tachibana, A., Yamada, S., and Kishimura, H. (2005) *Biosci Biotechnol. Biochem.* **69,** 2258–2262
8. Kondo, H., Morinaga, K., Misaki, R., Nakaya, M., and Watabe, S. (2005) *Gene* **346,** 257–266
9. Zhou, L., Wang, Y., Yao, B., Li, C. J., Ji, G. D., and Gui, J. F. (2005) *Comparative Biochem. Physiol.* **142,** 432–437
10. Choudhury, M., Yamada, S., Komatsu, M., Kishimura, H., and Ando, S. (2009) *Acta Biochim. Biophys Sin* **41,** 370–378
11. Provost, P. R., Boucher, E., and Tremblay, Y. (2009) *J. Endocrinol.* **200,** 321–330
12. Ishida, M., Ohashi, S., Kizaki, Y., Naito, J., Horiguchi, K., and Harigaya, T. (2007) *J. Reprod Dev.* **53,** 69–76
13. Poupard, G., André, M., Durliat, M., Ballagny, C., Boeuf, G., and Babin, P. J. (2000) *Cell Tissue Res.* **300,** 251–261
14. Montero, J. A., and Heisenberg, C. P. (2004) *Trends Cell Biol.* **14,** 620–627
15. Kimmel, C. B., and Law, R. D. (1985) *Dev. Biol.* **108,** 86–93
16. Trinkaus, J. P. (1993) *J. Exp. Zool* **265,** 258–284
17. Carvalho, L., Stühmer, J., Bois, J. S., Kalaidzidis, Y., Lecaudey, V., and Heisenberg, C. P. (2009) *Development* **136,** 1305–1315
18. D'Amico, L. A., and Cooper, M. S. (2001) *Dev. Dyn.* **222,** 611–624
19. Sakaguchi, T., Kikuchi, Y., Kuroiwa, A., Takeda, H., and Stainier, D. Y. (2006) *Development* **133,** 4063–4072
20. Yamanaka, Y., Mizuno, T., Sasai, Y., Kishi, M., Takeda, H., Kim, C. H., Hibi, M., and Hirano, T. (1998) *Genes Dev.* **12,** 2345–2353
21. Wilkins, S. J., Yoong, S., Verkade, H., Mizoguchi, T., Plowman, S. J., Hancock, J. F., Kikuchi, Y., Heath, J. K., and Perkins, A. C. (2008) *Dev. Biol.* **314,** 12–22
22. Fan, X., Hagos, E. G., Xu, B., Sias, C., Kawakami, K., Burdine, R. D., and Dougan, S. T. (2007) *Dev. Biol.* **310,** 363–378
23. Li, Z., Korzh, V., and Gong, Z. (2007) *BMC Dev. Biol.* **7,** 117
24. Ebert, A. M., McAnelly, C. A., Srinivasan, A., Linker, J. L., Horne, W. A., and Garrity, D. M. (2008) *Proc. Natl. Acad. Sci. U.S.A.* **105,** 198–203
25. Kikuchi, Y., Agathon, A., Alexander, J., Thisse, C., Waldron, S., Yelon, D., Thisse, B., and Stainier, D. Y. (2001) *Genes Dev.* **15,** 1493–1505
26. Ho, C. Y., Houart, C., Wilson, S. W., and Stainier, D. Y. (1999) *Curr. Biol.* **9,** 1131–1134
27. Westerfield, M. (1995) *The Zebrafish Book: A Guide for the Laboratory Use of Zebrafish (Danio rerio)*, M. Westerfield, Eugene, OR
28. Kimmel, C. B., Ballard, W. W., Kimmel, S. R., Ullmann, B., and Schilling, T. F. (1995) *Dev. Dyn.* **203,** 253–310
29. Thisse, C., and Thisse, B. (2008) *Nat. Protoc.* **3,** 59–69
30. Weiser, D. C., Row, R. H., and Kimelman, D. (2009) *Development* **136,** 2375–2384
31. Hirata, T., Yamanaka, Y., Ryu, S. L., Shimizu, T., Yabe, T., Hibi, M., and Hirano, T. (2000) *Biochem. Biophys. Res. Commun.* **271,** 603–609
32. Cheng, J. C., Miller, A. L., and Webb, S. E. (2004) *Dev. Dyn.* **231,** 313–323
33. Zalik, S. E., Lewandowski, E., Kam, Z., and Geiger, B. (1999) *Biochem. Cell Biol.* **77,** 527–542
34. Hancock, J. F., and Prior, I. A. (2005) *Methods* **37,** 165–172
35. Solnica-Krezel, L., and Driever, W. (1994) *Development* **120,** 2443–2455
36. Hsu, H. J., Liang, M. R., Chen, C. T., and Chung, B. C. (2006) *Nature* **439,** 480–483
37. Cooper, M. S., and Virta, V. C. (2007) *J. Exp. Zool B Mol. Dev. Evol.* **308,** 591–608
38. Chen, S., and Kimelman, D. (2000) *Development* **127,** 4681–4689
39. Lyman Gingerich, J., Lindeman, R., Putiri, E., Stolzmann, K., and Pelegri, F. (2006) *Dev. Dyn.* **235,** 2749–2760
40. Mizuno, T., Yamaha, E., Kuroiwa, A., and Takeda, H. (1999) *Mech. Dev.* **81,** 51–63
41. Trinh, L. A., and Stainier, D. Y. (2004) *Dev. Cell* **6,** 371–382
42. Weng, W., and Breslow, J. L. (1996) *Proc. Natl. Acad. Sci. U.S.A.* **93,** 14788–14794
43. Castellani, L. W., Goto, A. M., and Lusis, A. J. (2001) *Diabetes* **50,** 643–651
44. Castellani, L. W., Nguyen, C. N., Charugundla, S., Weinstein, M. M., Doan, C. X., Blaner, W. S., Wongsiriroj, N., and Lusis, A. J. (2008) *J. Biol. Chem.* **283,** 11633–11644